A Free-Space Optically Locked VCO With Picosecond Timing Jitter in 0.18-μm CMOS

Xuebei Yang, Xuyang Lu, and Aydin Babakhani

***Abstract*— In this letter, we present a novel receiver for time transfer that achieves picosecond accuracy through a line-of-sight link. The receiver is based on a fully integrated optically locked voltage controlled oscillator (OL-VCO) and is implemented in a commercial CMOS process. The design of optical photodiodes integrated with the OL-VCO is explained in detail. It is demonstrated that in the locked mode, the OL-VCO can be synchronized with a 1.3-GHz RF source through a free-space optical link. The free-space synchronization improves the phase noise of the OL-VCO by 25 dB at 100-Hz offset frequency. It is shown that a time transfer accuracy of picosecond can be achieved over a distance of 1.5 m. This represents more than two orders of magnitude improvement compared with the prior art.**

***Index Terms*— Oscillators, photodiodes, CMOS, VCO, injection locking, time transfer.**

I. Introduction

THERE is great interest in establishing precision time synchronization among widely-spaced elements. Precision synchronization can be used to transfer time/frequency to remote locations. It can also be used to synchronize the elements of a large phased array. In conventional schemes, synchronization is achieved through wired links, such as electrical wires, waveguides and/or optical fibers [1]–[4]. Unfortunately, a wired link limits the flexibility of the system, increases the latency, and cannot be used where elements are mobile relative to each other. In this case, a wireless link must be used to synchronize the elements.

In the prior art, wireless synchronization using microwave radiation and free-space optics has been demonstrated [5]–[11]. For example, a synchronization receiver using microwave radiation is reported in [5] with picosecond timing jitter. The receiver was implemented in a CMOS process technology and a link distance of 2.5mm was achieved by using an external power amplifier. At microwave frequencies, the radiation pattern usually has low directivity. Therefore, microwave-based solutions can have a larger operation angle, but they usually suffer from multi-path issues [12]. In a multi-path environment, due to time-varying electromagnetic scattering, both the amplitude and phase of the synchronization signal become noisy, resulting in a large timing jitter. In contrast, because of the high directivity of optical beams, multi-path effects are negligible. Therefore, a much cleaner synchronization signal can be recovered and the timing jitter will be smaller. In the prior art [6]–[11], a free-running electrical oscillator was synchronized using a free-space optical link, and a significant reduction in phase noise was observed. However, in [6]–[11], the receiver is implemented using discrete components and non-silicon materials. Unfortunately, these solutions are not compatible with CMOS-based integrated circuits and hence have limited applications.

Manuscript received January 22, 2014; revised March 7, 2014; accepted April 4, 2014. Date of publication April 14, 2014; date of current version May 16, 2014.

The authors are with the Department of Electrical and Computer Engineering, Rice University, Houston, TX 77005 USA (e-mail: aydin.babakhani@rice.edu).

Color versions of one or more of the figures in this letter are available online at http://ieeexplore.ieee.org.

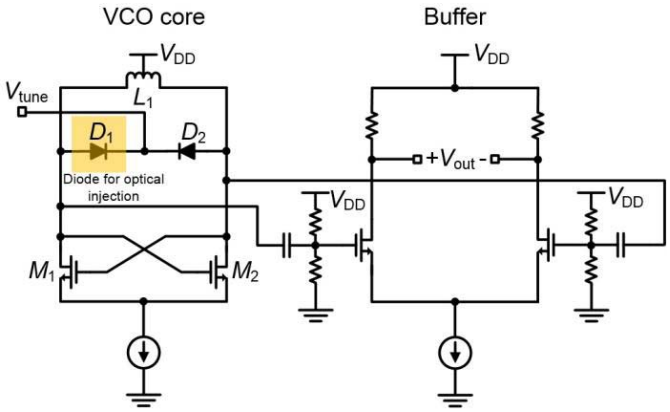

Fig. 1. The schematic of the OL-VCO with a differential buffer.

In this letter, for the first time, we report a fully-integrated CMOS-based Optically-Locked Voltage Controlled Oscillator (OL-VCO) that operates based on the concept of spatial injection locking. The chip is implemented using a commercial CMOS process technology without any post-processing and can be readily integrated with complex analog and digital circuits. The proposed OL-VCO has a free-running frequency around 1.3GHz. It can be tightly synchronized through a free-space optical beam at 850nm wavelength. The reported link achieves a picosecond timing jitter with distance of larger than one meter. To the best knowledge of the authors, this is the first demonstration of meter-range free-space synchronization with picosecond timing jitter using a fully-integrated CMOS receiver. It extends the previously reported 2.5mm range [5] by more than two orders of magnitude.

II. Operational Principle

The OL-VCO is implemented in a commercial 0.18μm CMOS SOI process technology. Figure 1 shows the schematic of the OL-VCO, which adopts a differential cross-coupled structure. The OL-VCO can operate in both free-running and locked modes. In the free-running mode, V_{tune} is set to be larger than V_{DD} so that the custom-designed diodes D_1 and D_2 are in the reverse bias region. The inductor L_1 resonates

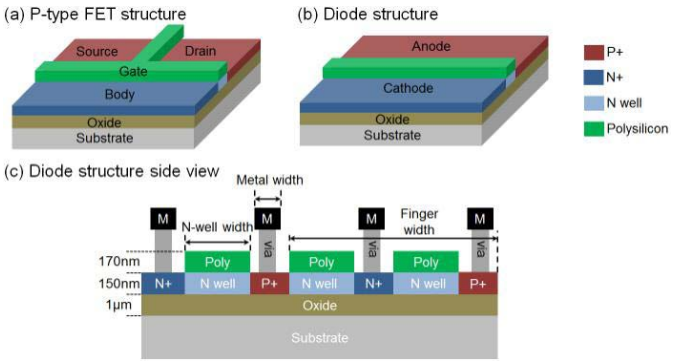

Fig. 2. The structure of (a) P-type FET with body contacts, and (b) diodes. The metal and vias are omitted. The silicon region covered by the polysilicon is N-well. (c) The side view of the diodes.

with capacitance of D_1 and D_2, while transistors M_1 and M_2 provide the negative resistance required for oscillation.

In an LC oscillator with a free-running frequency ω_0, the oscillation frequency can be locked to ω_{inj} if a current with frequency ω_{inj} is injected and ω_{inj} satisfies

$$|\omega_0 - \omega_{\text{inj}}| \leq \omega_L = \frac{\omega_0}{2Q} \cdot \frac{I_{\text{inj}}}{I_{osc}} \tag{1}$$

where Q is the quality factor of the LC tank. I_{inj} and I_{osc} are the injection current and the transistor current, respectively. ω_L is denoted as the locking range [13]. For a given oscillator with fixed I_{osc}, Q and ω_0, the injection current I_{inj} should be maximized to achieve a larger locking range.

III. The Design of Photodiodes

In this letter, we propose to inject the RF photo-current into the OL-VCO by illuminating the diode D_1, as highlighted in Figure 1. The implementation of photodiodes is a critical part in this design. In order to increase the locking range, the quantum efficiency of the photodiodes should be maximized at the desired frequency. However, several major challenges exist, limiting the efficiency of the photodiodes. First, in a commercial CMOS SOI process technology, there is no dedicated process to fabricate high-efficiency photodiodes. In this letter, the diodes provided by the foundry are based on the lateral body to source/drain junction of a P-type MOSFET, as shown in Figure 2. Second, in commercial CMOS processes such as the one used in this letter, key design parameters such as doping profiles are not disclosed by the foundry. Third, the foundry uses metal filling and enforces strict metal density requirements.

In order to overcome the above challenges, several approaches have been adopted. First, the metal filling above the diodes is blocked, and dummy metal structures are carefully added around the diodes to meet the metal density requirements. Second, in order to push the quantum efficiency, the layout of default diodes provided by the foundry is modified, and the layout impact of the photodiodes has been carefully analyzed. Three parameters studied are metal width, finger width, and N-well width, as annotated in Figure 2. Other parameters including the thickness of the silicon layer above the oxide are fixed by the foundry and cannot be

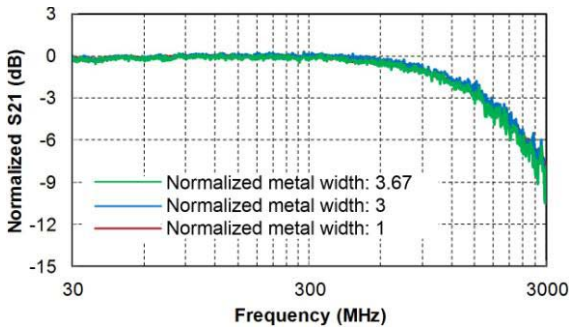

Fig. 3. The effects of metal width on the bandwidth for photodiodes.

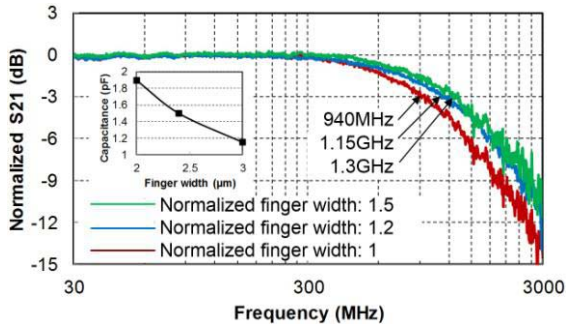

Fig. 4. The effects of finger width on the bandwidth of photodiodes.

varied. Various photodiodes with different layouts have been fabricated and their performance is measured. The dimensions are all kept at 50μm by 50μm to maintain a fair comparison. The diodes are biased at -3V. The photo-current is recorded to calculate the responsivity, while an Agilent network analyzer N5230C is used to measure the bandwidth [14].

We first study the effects of metal width. By reducing the metal width by 3.67×, it is observed that the responsivity increases by 3×, while the bandwidth is not affected, as shown in Figure 3. The contact resistance of the photodiode is calculated to be far less than 1Ω according to the datasheet provided by the foundry. Therefore, the contact resistance is negligible compared to the 50Ω load of the network analyzer, and does not affect the bandwidth in the measurement. Since metal layers block part of the optical beam, to maximize the quantum efficiency, their width should be kept at the minimum size allowed by the foundry.

We next study the effects of finger width. By varying the finger width, the N-well width is kept constant but the width of N+/P+ region changes. It is observed that as the finger width increases by 1.5×, the bandwidth of photodiodes increases by 25%, while the responsivity increases by 2.5×. The bandwidth improvement is attributed to the reduction in diode capacitance, as shown in Figure 4. In this letter, the total PN junction capacitance of the photodiode is the sum of the PN junction capacitance of all fingers. When the finger width increases, fewer fingers can be placed within a fixed width of 50μm. Since the PN junction capacitance for each finger does not change, the total PN junction capacitance decreases. Therefore, the RC time constant decreases and the bandwidth of photodiodes increases. Moreover, as the metal width remains constant for each finger, the percentage of the

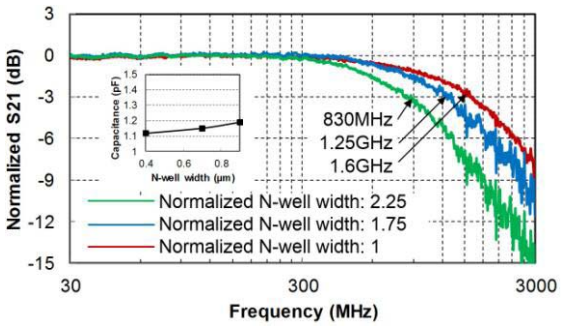

Fig. 5. The effects of N-well width on the bandwidth of photodiodes.

optical beam blocked by the metal layer decreases, which results in a higher responsivity.

We finally study the effects of N-well width. As the N-well width increases by 2.25×, the bandwidth reduces by 48%, while the responsivity increases by 1.5×. The bandwidth drop results from the inherent speed of the photodiode instead of the RC parasitics. As shown in Figure 5, the capacitance remains constant. For P+/N-well photodiodes studied in this work, the photocurrent is composed of the drift current in the depletion region, the electron diffusion current in the P+ region, and the hole diffusion current in the N-well. In this process, the diffusion length for holes in the N-well is estimated to be 10μm [15], which is much larger than the width of the N-well. Therefore, the majority of the holes generated in the N-well contribute to the total photocurrent. As the width of the N-well increases, the traveling time for holes to reach the depletion region increases, which reduces the bandwidth. On the other hand, as the width of N-well increases, more carriers can be collected. Hence, the responsivity increases. At 1.3GHz, it is calculated that photodiodes with the smallest N-well width have the largest quantum efficiency due to the largest bandwidth.

According to the measurement results of different photodiodes, we conclude that to maximize the quantum efficiency at 1.3GHz, the metal width, finger width, and N-well width should be set to 0.3μm, 1.8μm, and 0.4μm, respectively. The contact resistance of the optimized photodiode is calculated to be 0.2Ω. It achieves a 3dB bandwidth of 1.8GHz and responsivity of 0.005A/W at 850nm. The low responsivity of the photodiode is mainly caused by the thin absorption layer (150nm) that is fixed by the foundry. The second reason that reduces the responsivity is the reflection from the mandatory passivation layer in the CMOS process.

IV. Measurement Results

The micrograph of the fabricated OL-VCO is shown in Figure 6 (a). The supply voltage V_{DD} is kept at 1.3V. As V_{tune} increases from 2V to 6V, the capacitance of the diode reduces by 23%, and the free-running oscillation frequency of the OL-VCO increases from 1295MHz to 1381MHz. The increase in frequency is smaller than $1/\sqrt{1-0.23} = 14\%$ due to the capacitance of transistors and interconnects, which remain constant when varying V_{tune}. The output power is −8dBm across the frequency range.

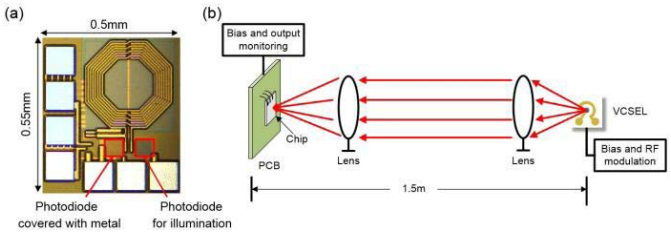

Fig. 6. (a) The micrograph of the fabrication OL-VCO chip. (b) The setup of the experiment. The focal length and diameter are 35mm and 25.4mm for both lenses.

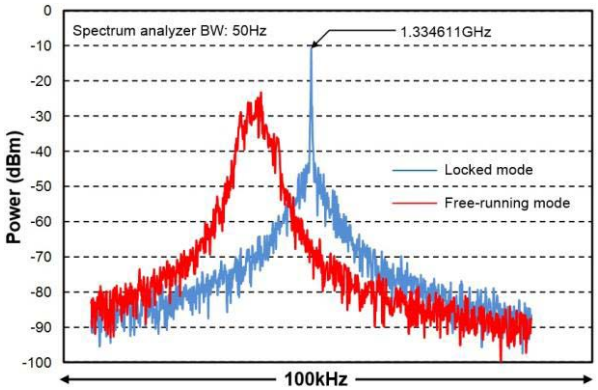

Fig. 7. The measured power spectrum of the OL-VCO in both free-running and locked modes.

A block diagram of the measurement setup for the OL-VCO in the locked mode is presented in Figure 6 (b). A directly-modulated Vertical Cavity Surface Emitting Laser (VCSEL) operating at 850nm with 11GHz bandwidth is used as the optical source. The amplitude of the optical signal is modulated by an Anritsu 68369B RF signal generator. The modulation frequency is close to the free-running frequency of the OL-VCO. In this letter, the laser beam is collimated and focused onto the photodiode of the OL-VCO through two discrete lenses. The lenses can be potentially removed if a laser source with higher power is used. It may also be integrated onto the same CMOS chip, as CMOS processes with integrated microlenses have recently been reported [16]. The distance between the VCSEL and the OL-VCO chip is 1.5 meters.

Figure 7 presents the output spectrum of OL-VCO in both free-running and locked modes, which is measured by an Agilent N9030A signal analyzer. The supply and tuning voltages are kept constant at 1.3V and 5.5V, respectively. The RF power of the laser beam is −3dBm. Based on Figure 7, it is clear that the OL-VCO in the locked mode generates a sharp tone at the injected frequency. Figure 8 shows the phase noise measurement results of the OL-VCO in both free-running and locked modes. At a reverse bias of −4.2V and RF laser power of −3dBm, the measured phase noise of the OL-VCO in the free-running mode at 100Hz and 1kHz offset from the carrier frequency is −32dBc/Hz and −40.3dBc/Hz, respectively. These values improve to −57dBc/Hz and −66.5dBc/Hz in the locked mode. Based on these measured values, the phase noise improves by about 25dB. The calculated rms jitter by integrating the phase noise from 100Hz to 1MHz is 81psec and 3.1psec for the OL-VCO in the free-running and locked modes, respectively. An Agilent DCA-X 86100D sampling

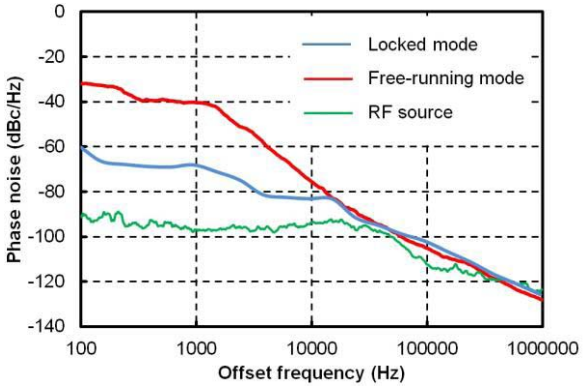

Fig. 8. The measured phase noise of the OL-VCO in both free-running and locked modes. The photodiode is biased at −4.2V, and the RF laser power is −3dBm.

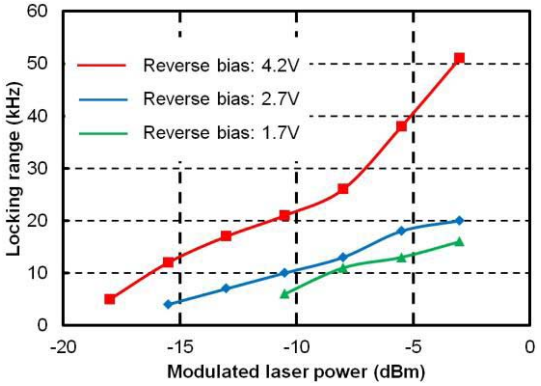

Fig. 9. Locking range of the OL-VCO as a function of the laser power and the bias of the photodiode. The DC laser power is fixed at 0 dBm.

oscilloscope is also used to measure the timing jitter for the OL-VCO in the locked mode. The measured rms jitter is 1.56psec with 16 averaging. In order to make sure that the locking is not due to RF radiation leakage, the laser beam is blocked and it is confirmed that no locking can be achieved afterward. To the best knowledge of the authors, this is the first demonstration of CMOS wireless synchronization with picosecond timing jitter at a distance larger than one meter.

We have also investigated the locking range of the OL-VCO. According to Equation (1), the locking range is proportional to the injection current. Therefore, the laser power directly influences the locking range. The reverse bias of the photodiode also impacts the injection current because a higher reverse bias leads to larger quantum efficiency. The measured locking range for different RF laser power and reverse biases is shown in Figure 9. It is confirmed that the locking range drops as the laser power and reverse bias decreases. The locking range can be potentially improved by further optimizing the photodiode, and amplifying the photo-current before injecting to the OL-VCO.

In Figure 10, the measured phase noise of the OL-VCO in the locked mode is presented under different photodiode biases and RF laser power. In an injection-locked VCO, the improvement of phase noise over the free-running VCO is more profound as the injection current increases [13]. As the larger reverse bias and higher input laser power increases the injection current, the phase noise of the OL-VCO drops, as is evident in Figure 10.

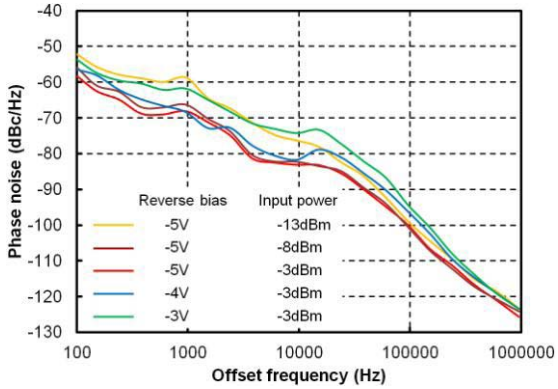

Fig. 10. The measured phase noise under different reverse biases and RF laser power.

V. Conclusion

In this letter, we present a CMOS OL-VCO implemented on a single chip. Although a CMOS SOI process is used, the OL-VCO can be implemented in bulk CMOS processes as well, provided that an efficient and fast photo-detector can be implemented. By optimizing the photodiode layout and circuit structure of the OL-VCO, wireless synchronization with picosencond timing jitter at transmitter-receiver distance of 1.5m is achieved.

References

[1] P. Moreira, J. Serrano, T. Wlostowski, P. Loschmidt, and G. Gaderer, "White rabbit: Sub-nanosecond timing distribution over ethernet," in *Proc. ISPCS Meas., Control Commun.*, Oct. 2009, pp. 1–5.

[2] D. Parker and D. C. Zimmermann, "Phased arrays-part II: Implementations, applications, and future trends," *IEEE Trans. Microw. Theory Tech.*, vol. 50, no. 3, pp. 688–698, Mar. 2002.

[3] A. Nejadmalayeri *et al.*, "Integrated optical phase lock loop," in *Proc. CLEO*, 2011.

[4] M. Peng *et al.*, "Long-term stable, sub-femtosecond timing distribution via a 1.2-km polarization-maintaining fiber link: Approaching 10^{-21} link stability," *Opt. Exp.*, vol. 21, no. 17, pp. 19982–19989, 2013.

[5] X. Guo, D. Yang, R. Li, and K. K. O, "A receiver with start-up initialization and programmable delays for wireless clock distribution," in *IEEE ISSCC Dig. Tech. Papers*, Feb. 2006, pp. 386–387.

[6] H. W. Yen and M. K. Barnoski, "Optical injection locking and switching of transistor oscillators," *Appl. Phys. Lett.*, vol. 32, no. 3, pp. 182–184, 1978.

[7] A. A. A. de Salles and J. R. Forrest, "Initial observations of optical injection locking of GaAs metal semiconductor field effect transistor oscillators," *Appl. Phys. Lett.*, vol. 38, no. 5, pp. 392–394, 1981.

[8] A. A. A. De Salles, "Optical control of GaAs MESFET's," *IEEE Trans. Microw. Theory Tech.*, vol. 31, no. 10, pp. 812–820, Oct. 1983.

[9] A. J. Seeds and A. A. A. De Salles, "Optical control of microwave semiconductor devices," *IEEE Trans. Microw. Theory Tech.*, vol. 38, no. 5, pp. 577–585, May 1990.

[10] A. S. Daryoush, "Optical synchronization of millimeter-wave oscillators for distributed architecture," *IEEE Trans. Microw. Theory Tech.*, vol. 38, no. 5, pp. 467–476, May 1990.

[11] J. Kim, F. X. Kärtner, and M. H. Perrott, "Femtosecond synchronization of radio frequency signals with optical pulse trains," *Opt. Lett.*, vol. 29, no. 17, pp. 2076–2078, 2004.

[12] W. Jakes, *Microwave Mobile Communications*. Hoboken, NJ, USA: Wiley, 1994.

[13] B. Razavi, "A study of injection locking and pulling in oscillators," *IEEE J. Solid-State Circuits*, vol. 39, no. 9, pp. 1415–1424, Sep. 2004.

[14] X. Yang, X. Lu, and A. Babakhani, "Impact of layout on the performance of photodiodes in 0.18 μm CMOS SOI," in *Proc. IEEE Photon. Conf.*, Sep. 2013, pp. 586–587.

[15] F. Tavernier and M. Steyaert, *High-Speed Optical Receivers With Integrated Photodiode in Nanoscale CMOS*. New York, NY, USA: Springer-Verlag, 2011.

[16] M. Cohen *et al.*, "Fully optimized Cu based process with dedicated cavity etch for 1.75 μm and 1.45 μm pixel pitch CMOS image sensors," in *Proc. IEEE IEDM*, Dec. 2006, pp. 1–4.